International Journal of Nanomedicine

Dovepress
open access to scientific and medical research

Open Access Full Text Article

ORIGINAL RESEARCH

Zinc oxide nanoparticles-induced epigenetic change and G2/M arrest are associated with apoptosis in human epidermal keratinocytes

This article was published in the following Dove Press journal:
International Journal of Nanomedicine
11 August 2016
Number of times this article has been viewed

Fei Gao
Ningjie Ma
Hong Zhou
Qing Wang
Hao Zhang
Pu Wang
Haoli Hou
Huan Wen
Lijia Li

State Key Laboratory of Hybrid Rice, College of Life Sciences, Wuhan University, Wuhan, People's Republic of China

Abstract: As an engineered nanomaterial, zinc oxide nanoparticles (ZnO NPs) are used frequently in biological applications and can make contact with human skin. Here, we systematically investigated the effects of ZnO NPs on non-tumorigenic human epidermal keratinocytes, which were used as a test model for this in vitro study, at the epigenetic and molecular levels. Our results showed that ZnO NPs induced cell cycle arrest at the G2/M checkpoint before the viability of human epidermal keratinocytes was reduced, which was associated with the chromatin changes at the epigenetic level, including increased methylation of histone H3K9 and decreased acetylation of histone H4K5 accompanied by chromatin condensation at 24 hours. The mRNA expression of the methyltransferase genes *G9a* and *GLP* was also increased upon treatment with ZnO NPs, and the acetyltransferase genes *GCN5*, *P300*, and *CBP* were downregulated. Reactive oxygen species were found to be more abundant after treatment with ZnO NPs for 6 hours, and DNA damage was observed at 24 hours. Transmission electron microscopy and flow cytometry confirmed that ZnO NPs were absorbed into the cell when they were added to the medium. Apoptotic human epidermal keratinocytes were detected, and the expression of the proapoptotic genes *Bax*, *Noxa*, and *Puma* increased significantly, while the expression of the antiapoptotic gene *Bcl-xl* decreased 24 hours after exposure to ZnO NPs. These findings suggest that the ZnO NPs induced cell cycle arrest at G2/M, which was associated with epigenetic changes and accompanied by p53-Bax mitochondrial pathway-mediated apoptosis.

Keywords: ZnO nanoparticle, cell cycle G2/M arrest, histone modification, p53-Bax mitochondrial apoptosis pathway, reactive oxygen species

Introduction

Zinc oxide nanoparticles (ZnO NPs) have been widely used in various biological fields, such as in cosmetics, as food additives, and for drug delivery, cell imaging, and cancer therapy.[1,2] ZnO NPs are added to sunscreens and facial creams to provide protection against skin damage by ultraviolet-A irradiation.[3,4] Their nanoscale size confers to them unique physical, chemical, and biological properties and functionality. An understanding of the behavior and genetic effects of nanoparticles (NPs) in living systems is vital for both the design of functionalized NPs and the application of nanomaterial-based formulation of medicines already in use.

Previous studies have demonstrated that ZnO NPs cause cyto- and genotoxicity in vivo or in vitro, accompanied by inflammation, reduced cell viability, DNA damage, and apoptosis. For example, ZnO NPs induced immunotoxicity in murine macrophages (RAW264.7 cells)[5] and mice.[6] ZnO NPs also induced cell toxicity and apoptosis in malignant human skin melanoma cells and in respiratory disease patients through

Correspondence: Lijia Li
State Key Laboratory of Hybrid Rice, College of Life Sciences, Wuhan University, 299 Bayi Road, Wuchang District, Wuhan 430072, People's Republic of China
Tel/fax +86 27 6875 4505
Email ljli@whu.edu.cn

submit your manuscript | www.dovepress.com
Dovepress
http://dx.doi.org/10.2147/IJN.S107021

the generation of reactive oxygen species (ROS), DNA damage, and p53 signaling pathway activation.[7,8] Previous studies have reported that ZnO NPs cause selective toxicity to cancer cells by apoptosis via lipid peroxidation[9] and ROS generation.[10] Long-term exposure to ZnO NPs has been reported to stimulate the generation of ROS, initiating death processes and affecting the cell cycle distribution.[11] ZnO NPs may inhibit cell growth by reducing proliferation.[12,13] Reduced proliferation has been linked to cell cycle arrest at various phases.[11,14,15] Cell cycle progression is blocked in response to diverse internal and external cues. The tumor suppressor p53 is able to activate G2/M cell cycle checkpoints, DNA repair, and apoptotic responses to maintain genomic stability.[16]

Instead of studying the reduced viability of cells associated with the cyto- and genotoxicity of ZnO NPs, we focused on the epigenomic response involved in cell cycle arrest at the G2/M checkpoint before the reduction in the viability of cells occurs. Chromatin can be modified through methylation of cytosine in DNA and posttranslational modifications of histones at lysine residues including acetylation, phosphorylation, and methylation, all of which may be involved in regulating gene expression.[17] Understanding the specific epigenomic response will provide new insights into gene regulation and its role in cellular growth, differentiation, cell death, diseases, and aging.[18] Epigenomic mechanisms have emerged as a new mediator of the interaction between the environment and chromatin.[19] Pan et al reported that Gd metallofullerenol nanomaterials inhibit pancreatic cancer metastasis by suppressing the interaction of histone deacetylase 1 with metastasis-associated proteins.[20] However, the epigenomic response involved in cell cycle arrest and the subsequent reduction in cell viability induced by ZnO NPs have not been reported.

The particle size and morphology, the functional groups on the NP surface, and the cell type have been shown to determine the subcellular distribution of NPs and are associated with variable toxicity and subsequent cell fate.[21] Kodiha et al reported that the different subcellular distributions of different gold nanoparticles (Au NPs) could cause tumor cell death by photothermal ablation, mechanical damage, and an increase in the localized drug concentration.[22] Ultrasmall Au NPs used as carriers for nucleus-based gene therapy have size-dependent effects.[23] The application of ZnO NPs with a size of 100 nm is generally recognized as safe by the US Food and Drug Administration due to their better biocompatibility than smaller ZnO NPs, and NPs of such size can be delivered into cells and can accumulate in different subcellular organelles.[24] HaCaT cells are non-tumorigenic human epidermal keratinocytes[25] that are reported to have normal p53 activity, and for this reason, have been widely used to study cell cycle alterations and mechanisms involved in NP-induced toxicity.[26,27]

Because humans are often directly exposed to ZnO NPs, it seems logical that the skin would act as a major target for ZnO NPs before they gain entry into the body through any of the possible routes. Therefore, the aim of the present study was to assess the epigenomic response involved in cell cycle arrest and to understand the mechanism involved in the subsequent relevant apoptotic routes in HaCaT cells after exposure to ZnO NPs. The present study found that ZnO NPs delayed the cell cycle at the G2/M checkpoint, which was followed by reduced HaCaT cell viability. Increased methylation of histone H3K9, decreased acetylation of histone H4K5, and condensed chromatin were observed through Western blotting and immunostaining analysis, accompanied by elevated levels of mRNA of the methyltransferase genes *G9a* and *GLP* and reduced expression of the acetyltransferase genes *GCN5*, *P300*, and *CBP*, after treatment with ZnO NPs. The production of ROS was found to be increased, and DNA damage was observed following treatment with ZnO NPs. Transmission electron microscopy (TEM) and flow cytometry confirmed that ZnO NPs were absorbed into the cell. Apoptotic HaCaT cells were studied, and the expression of the proapoptotic genes *Bax*, *Noxa*, and *Puma* was found to increase significantly, whereas the expression of the antiapoptotic gene *Bcl-xl* was found to decrease, after exposure to ZnO NPs. Our findings suggested that ZnO NPs induced cell cycle arrest at G2/M that was associated with epigenetic changes and accompanied by p53-Bax mitochondrial pathway-mediated apoptosis.

Materials and methods

Characterization of ZnO NPs

ZnO NPs (<100 nm; 99.7% metal basis; specific surface area, 15–25 m^2/g) were purchased from Sigma-Aldrich Co. (St Louis, MO, USA). For scanning electron microscopy (SEM) (S3400N; Hitachi, Tokyo, Japan) analysis, the samples were fixed onto metallic studs with double-sided conductive tape and sputtered with gold. SEM micrographs were analyzed with ImageJ (National Institutes of Health, Bethesda, MD, USA) software to obtain the mean size of pristine ZnO NPs. The hydrodynamic size and zeta potential of ZnO NPs in cell culture medium were determined by dynamic light scattering (DLS) (ZetaSizer-HT; Malvern Instruments, Malvern, UK). The samples of ZnO NPs in powder form

were suspended in cell culture medium at a concentration of 1 mg/mL and were sonicated in a water bath at 4°C for 30 minutes at 30 W to form a homogeneous suspension. This stock solution of ZnO NPs was diluted to a 10–100 μg/mL working solution for DLS size measurement.

Antibodies

The following antibodies were used for immunostaining and western blotting. Anti-H4K5ac (07-327), anti-H3K9me2 (05-1249), anti-H3 (06-755), and fluorescein-conjugated goat anti-rabbit IgG (12-507) antibodies were obtained from EMD Millipore (Billerica, MA, USA). The anti-γ-H2AX (ab2893) was purchased from Abcam (Cambridge, UK). The alkaline phosphatase-conjugated goat anti-rabbit IgG (A4187) was obtained from Sigma-Aldrich Co.

Cell culture

HaCaT cells (cell line GDC106; China Center for Type Culture Collection, Wuhan University, People's Republic of China) were seeded in α-minimal essential medium (Hyclone™; Thermo Fisher Scientific, Waltham, MA, USA) supplemented with 10% (v/v) fetal bovine serum (Hyclone™, Thermo Fisher Scientific) and maintained in a humidified environment at 5% CO_2 and 37°C.

Cell viability analysis

Cell viability was measured by the MTS (3-(4,5-dimethylthiazol-2-yl)-5-(3-carboxymethoxyphenyl)-2-(4-sulfophenyl)-2*H*-tetrazolium; inner salt) assay. HaCaT cells were seeded in a 96-well cell culture plate with 1×10^4 cells in 100 μL medium per well. After 12 hours, the cells were exposed to ZnO NPs at different concentrations (0, 0.5, 5, 10, 15, 20, 50, 100, and 200 μg/mL) and then cultured for 24, 48, and 72 hours, respectively. At the end of exposure, 20 μL MTS solution (Promega Corporation, Fitchburg, WI, USA) was added to every well, and the cells were incubated for 4 hours at 37°C. According to the manufacturer's protocol, the assay is based on conversion of MTS into the soluble, colored formazan product by mitochondrial dehydrogenase in metabolically active cells. Absorbance was quantified at 490 nm with a microplate spectrophotometer system (ELx800; BioTek, Winooski, VT, USA). The viability of treated groups was expressed as the absorbance ratio of the treated groups to that of the control group: cell viability = $(A_T - A_{T1})/(A_C - A_{C1})$, where A_T is the absorbance of the treated group, A_{T1} is the absorbance of a suspension of ZnO NPs in cell-free medium, A_C is the absorbance of the control group, and A_{C1} is the absorbance of cell-free medium.

Flow cytometry

Cell cycle analysis

The cell cycle distribution was analyzed by flow cytometry. Untreated HaCaT cells or cells treated with ZnO NPs were trypsinized and counted. Then, 5×10^5 cells were fixed in ethanol at −20°C overnight, resuspended in 1× phosphate-buffered saline (PBS; pH 7.4), and incubated with DNase-free RNase A (Thermo Fisher Scientific) and propidium iodide (PI; Thermo Fisher Scientific) for 1 hour at 37°C in the dark. Fluorescence was measured at 585 nm with a FACSCalibur flow cytometer (Becton Dickinson, San Jose, CA, USA), and 10,000 cells were collected for each analysis. The results of flow cytometry were quantified using the software Summit 4.3 (Beckman Coulter Inc., Brea, CA, USA).

Cellular uptake with ZnO NPs analysis

The uptake of ZnO NPs was examined by analyzing forward scatter versus side scatter (SSC) using flow cytometry as described previously.[28] Briefly, cells were incubated with 20 or 50 μg/mL ZnO NPs for 24 hours in the α-minimal essential medium, and then they were suspended in PBS for flow cytometry. Following this, the control and ZnO NPs-exposed cells were analyzed with the flow cytometer, with increases in the SSC due to endocytotic or adsorptive NP interactions. The results of flow cytometry were quantified using the software Summit 4.3 (Beckman Coulter Inc.).

ROS formation analysis

ROS were measured by the fluorescent probe 2′,7′-dichlorodihydrofluorescein diacetate (Sigma-Aldrich Co.). Cells were incubated at 37°C with ZnO NPs for 0, 6, or 24 hours, or 10 days. After treatment, cells were washed with PBS and then incubated at 37°C with 2′,7′-dichlorodihydrofluorescein diacetate in serum-free medium for 30 minutes. The ROS-linked fluorescence, with emission at 525 nm, was quantified by flow cytometry. The results of flow cytometry were quantified using Summit 4.3 (Beckman Coulter Inc.) and FlowJo 7.6 (Tree Star Inc., Ashland, OR, USA).

Apoptosis analysis

Flow cytometry was used to measure Annexin V-fluorescein isothiocyanate (FITC)/PI staining to investigate the mode of cell death induced by ZnO NPs. Annexin V-FITC/PI staining was carried out with an Annexin V-FITC apoptosis detection kit (Beyotime, Haimen, People's Republic of China). Briefly, the cells were harvested by trypsinization, washed with PBS, and resuspended in binding buffer

(10 mM (4-(2-hydroxyethyl)-1-piperazineethanesulfonic acid)/NaOH, pH 7.5, containing 140 mM NaCl and 2.5 mM $CaCl_2$) at a concentration of 10^6 cells/mL. Annexin V-FITC (5 µL) and PI (10 µL) were added to 195 µL of the cell suspension and incubated for 20 minutes in the dark at room temperature. The cells were immediately analyzed by flow cytometry. Fluorescence emitted by Annexin V-bound FITC and DNA-bound PI was detected as green and red fluorescence, respectively. The results were analyzed by software Summit 4.3 (Beckman Coulter Inc.).

Transmission electron microscopy

Dispersed samples were dropped onto carbon-coated copper grids and viewed under a transmission electron microscope (HIH-8100; Hitachi) at an accelerating voltage of 200 kV. TEM photomicrographs were analyzed by ImageJ (National Institutes of Health) to assess the location of ZnO NPs in HaCaT cells and the mean size of ZnO NP aggregates (n=50).

Scanning electron microscopy

For SEM, cells were grown on glass slides and treated with ZnO NPs for 24 hours. After exposure, cells were fixed with 1% paraformaldehyde, dehydrated in 25%, 50%, 75%, 80%, 90%, and 100% ethanol, lyophilized for 4 hours, coated with gold, and examined with a scanning electron microscope (S3400N; Hitachi). SEM photomicrographs were analyzed by ImageJ (National Institutes of Health) to assess the morphology of the HaCaT cell surface.

Histone extraction

After 24 hours of exposure to ZnO NPs, cells were collected and washed twice with 1X PBS. Cells were lysed in extraction buffer (100 mM Tris–HCl, pH 7.4, containing 4% sodium dodecyl sulfate, 20% glycerinum, 200 mM dithiothreitol, and 1 mM phenylmethanesulfonyl fluoride). The protein concentration was determined using a DC Protein Kit Assay (Bio-Rad Laboratories Inc., Hercules, CA, USA).

Western blotting

Western blotting was carried out as previously described.[29] Histone H3 was used as an equal loading control.

Immunostaining

HaCaT cells were plated at a density of 5×10^4 cells on glass coverslips in a 12-well plate and treated under different conditions. Cells on coverslips were fixed for 20 minutes with fresh 4% paraformaldehyde and then incubated with 0.5% Triton X-100 (Sigma-Aldrich Co.). The cells were incubated with primary antibodies at 4°C overnight, followed by 2 hours of incubation at 37°C with secondary antibodies conjugated to FITC. DNA in the cell nucleus was stained with 0.2 µg/mL 4,6-diamidino-2-phenylindole (Sigma-Aldrich Co.). Images were captured with a fluorescence microscope (BX-60; Olympus, Tokyo, Japan) equipped with the CCD monochrome camera Sensys 1401E and pseudo-colored using the software MetaMorph 7.7.2 (Universal Imaging Corp, Downingtown, PA, USA). The microscope settings and exposure times were kept constant for each respective channel (4,6-diamidino-2-phenylindole or FITC). More than 500 nuclei were analyzed for each treatment group.

Reverse transcription and quantitative real-time PCR

Quantitative real-time polymerase chain reaction (PCR) primers were designed with primer Premier 5 software (PREMIER Biosoft International, Palo Alto, CA, USA) (Table 1). β-Actin was used as the reference gene, and all of the PCR products were ~200 bp. Total RNA was isolated by TRIzol reagent (Thermo Fisher Scientific), and 1 µg of total RNA was reverse-transcribed into cDNA with the RevertAid First Strand cDNA Synthesis Kit (Fermentas). Quantitative real-time PCR was carried out using SYBR Green Real-time PCR Master Mix (Toyobo, Tokyo, Japan) on the ABI StepOnePlus real-time PCR system (Thermo Fisher Scientific).

Table 1 Primers used for real-time PCR

Primer	Sequences (5′–3′)
G9a	AGCTTCCGAAGATAGAACGAG
	ACAGGGGTTGGGTAGATACTC
GLP	TCAGGAGAGATACAGCCAGG
	TTGCTGGCGATGAGAGAAGT
GCN5	ACCTCTATCAAGCAGCTCCTCCG
	AGTTTAGCTCACCCTCCTCAAT
P300	CAATGTGATCCATGGCGAGA
	ATGCATGTTTCATCCCCACT
CBP	GTGCAGGCTCAGTCCCTAAC
	GGGTGTCCATATGGTCTTGT
Bax	GTCGTCTTCTCTATTTTGC
	GCAGCAAGTCTAATGTGCAG
Bcl-2	CGAGGACTTCACCGGCGGCAAGCGC
	CCGCATCCTGGGGGCGTACTGTTCC
Bcl-xl	CCCACAATGGAAACACCTGG
	GCGTTCCGTGTCTCCATTAC
Noxa	GTGGCCTTCGATACGCAAGA
	CCAGGCGCGCAGTCAAATCA
Puma	TTGTCTGCACGATGTTGCATTCTGGA
	GCCAGGGCCAGTCTCTAGGA
Hsp70	TCAGGACTCAATCTGCATCG
	ATCCGCATTTCTGGTTATCA
β-Actin	AAGAGCAATGACCTGCGTGA
	ACGGAAGTCAAGGTCACTCT

Abbreviation: PCR, polymerase chain reaction.

The PCR amplification conditions were 95°C for 2 minutes, followed by 40 cycles of 5 seconds at 95°C, 56°C for 15 seconds, and 72°C for 20 seconds. The threshold cycle number for each PCR product was estimated, and the relative expression levels for genes were obtained using the $2^{-\Delta\Delta Ct}$ method with the StepOne software version 2.1 (Thermo Fisher Scientific). Experiments were performed in triplicate biological replicates.

Results

ZnO NPs inhibited HaCaT cell growth

To characterize the physical features of ZnO NPs, SEM and DLS were employed to analyze these materials. As seen in Figure 1, ZnO materials formed rod-shaped particles (Figure 1A), and DLS characterization revealed that the ZnO particles in dispersion had an average size of 132.55±0.45 nm and a zeta potential of −12.6±0.95 mV (Figure 1B). Next, a viability assay was performed to determine the effect of these ZnO NPs on HaCaT cells. The results showed that the viability of HaCaT cells decreased with increasing concentrations of ZnO NPs (Figure 2A). The cell viability at 48 and 72 hours was clearly reduced at concentrations >15 μg/mL from 80% at 20 μg/mL to 60% at 50 μg/mL, while at 24 hours, no obvious difference in cell viability was seen between the 20 and 50 μg/mL treatment groups. Images (Figure 2B) of cell culture also showed that the number of cells decreased with increasing ZnO NP concentration after treatment for 48 hours, which was consistent with the results of the MTS assay.

ZnO NP treatment induced cell cycle arrest at the G2/M phase in HaCaT cells

The ZnO NP treatment-induced decrease in cell viability led to us to examine whether cell cycle alterations were induced by ZnO NPs before the decrease in cell viability was observed. We examined the cell cycle distribution of HaCaT cells after 24 hours of exposure to ZnO NPs at 20 and 50 μg/mL by flow cytometry (Figure 2C). Compared with the control, a clearly increased portion of cells treated with 50 μg/mL (Figure 2D) were in the G2/M phase. After treatment with 50 μg/mL, 33.55% of cells were in G2/M, in contrast to 16.65% of the control cells. The portion of cells in the S phase at 50 μg/mL was 22.33%, which was clearly less than that of the control (38.83%). The data suggested that ZnO NPs induced cell cycle arrest at the G2/M phase. The expression of specific marker genes *CyclinB1* and *CDK1* was decreased after treatment with 20 or 50 μg/mL ZnO NPs, indicative of cell cycle arrest at G2/M, and the expression of *PCNA*, a marker of cell proliferation, also decreased after ZnO NP treatment (Figure 2E).

H4K5ac levels decreased and H3K9me2 levels increased in HaCaT cells after exposure to ZnO NPs

It has been demonstrated that chromatin histone modification is involved in the changes in chromatin structure and cell cycle progression during mitosis.[30,31] Thus, histone modification levels were analyzed after treatment with ZnO NPs. Upon treatment with ZnO NPs for 24 hours, chromatin condensation was observed, and the nucleus became smaller (Figure 3A). The number of condensed nuclei increased with increasing concentration of ZnO NPs. The number of moderately condensed nuclei was nearly 3.5-fold higher in treated groups than in the control group; the smallest condensed nuclei only occurred with 50 μg/mL of treatment, but the group treated with 20 μg/mL and the control group both showed no nuclei that had condensed to the smallest size (Figure 3A). ZnO NPs could also induce changes at the epigenetic level in nuclei.

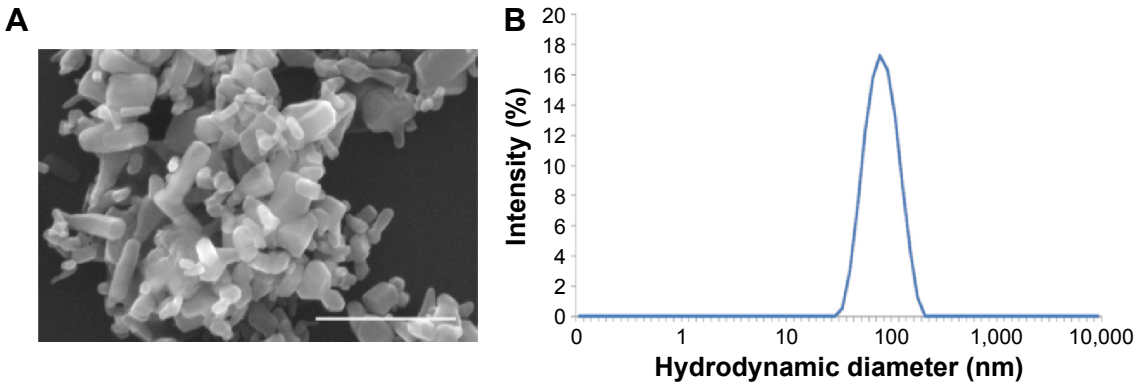

Figure 1 Characterizations of ZnO NPs.
Notes: (**A**) Scanning electron microscopy image of ZnO NPs; scale bar =500 nm. (**B**) Hydrodynamic diameter.
Abbreviation: ZnO NPs, zinc oxide nanoparticles.

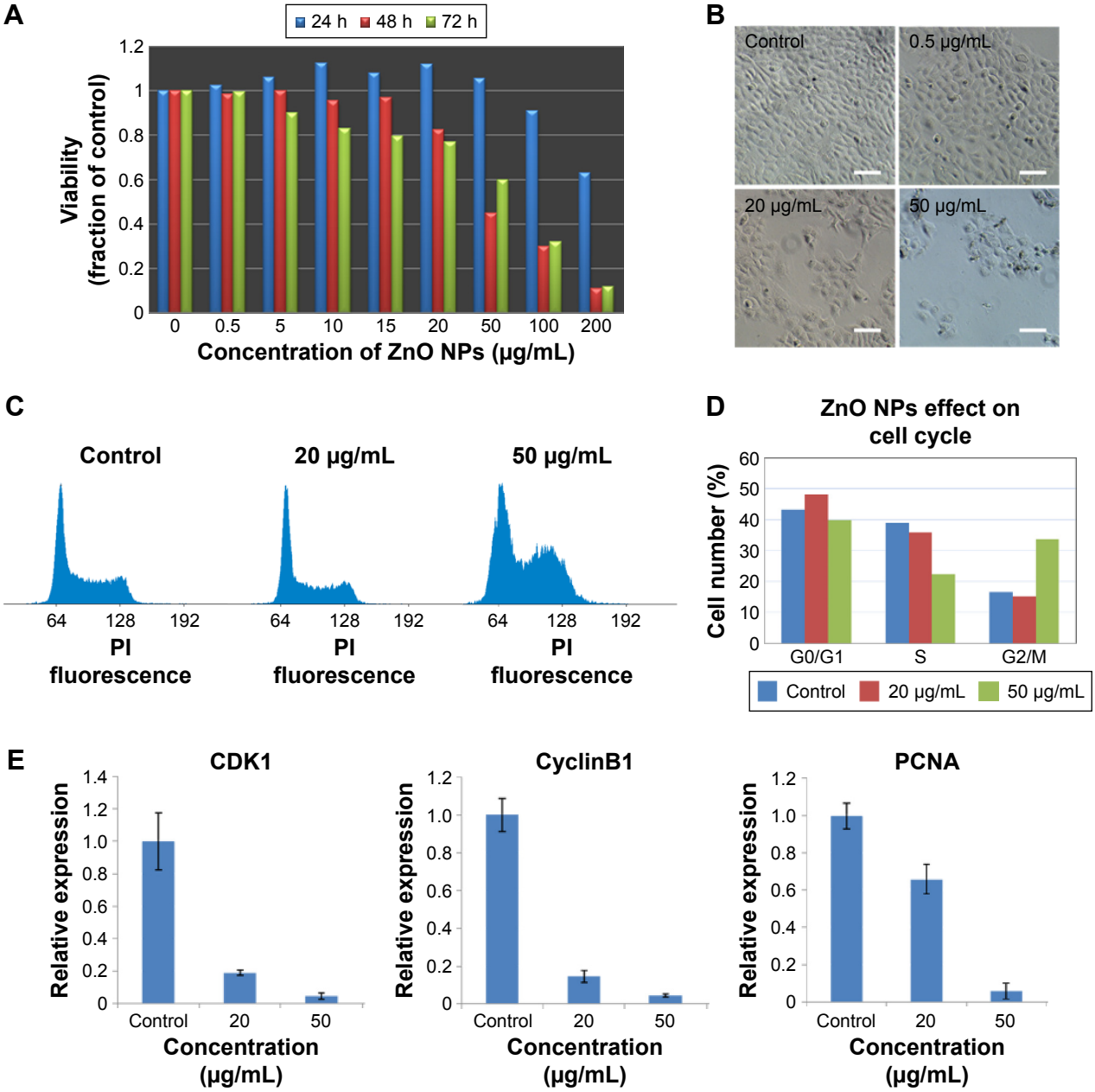

Figure 2 Viability of HaCaT cells and cell cycle alterations in HaCaT cells after exposure to ZnO NPs.

Notes: (**A**) Viability of HaCaT cells treated with ZnO NPs at different concentrations for 24, 48, and 72 hours. (**B**) Images of HaCaT cells in cell cultures treated without or with ZnO NPs at 0.5, 20, and 50 μg/mL for 48 hours monitored by an inverted phase-contrast microscope. Scale bars =40 μm. (**C**) Flow cytometry analysis of cell cycle change. The propidium iodide, a DNA-specific intercalating dye, was used to stain cells. 64: diploid cells with one-chromatid chromatin (G1 phase); 128: diploid cells with two chromatid chromatin (G2/M phase). (**D**) The quantitative analysis of cells at different phases based on flow cytometry data. The results showed that ZnO NP treatment caused the cell cycle arrest in G2/M checkpoint. (**E**) The expression of specific marker genes *CyclinB1* and *CDK1* in G2/M cell cycle arrest was decreased, and the expression of *PCNA* which was used for estimating cell proliferation was decreased in HaCaT cells after exposure to ZnO NPs for 24 hours as measured by real-time PCR.

Abbreviations: ZnO NPs, zinc oxide nanoparticles; PCR, polymerase chain reaction; PI, propidium iodide; h, hours.

Histone acetylation is always related to the decondensed chromatin state and gene activation, whereas deacetylation is a marker of chromatin condensation and gene silencing.[17] As expected, Western blot analysis (Figure 3C and D) showed that H4K5ac levels were fourfold lower with increasing ZnO NP concentrations; by contrast, H3K9me2 signals were nearly 1.5-fold higher, although after exposure to ZnO NPs at 0.5 μg/mL, H3K9me2 signals were slightly lower. Immunostaining analysis (Figure 3B) showed increased H3K9me2 signals which were mainly distributed in heterochromatin regions after exposure to 20 or 50 μg/mL ZnO NPs. Epigenetic modifications are regulated by enzymes. The data presented by Figure 3E showed that the expression of histone methyltransferase genes was increased after treatment with

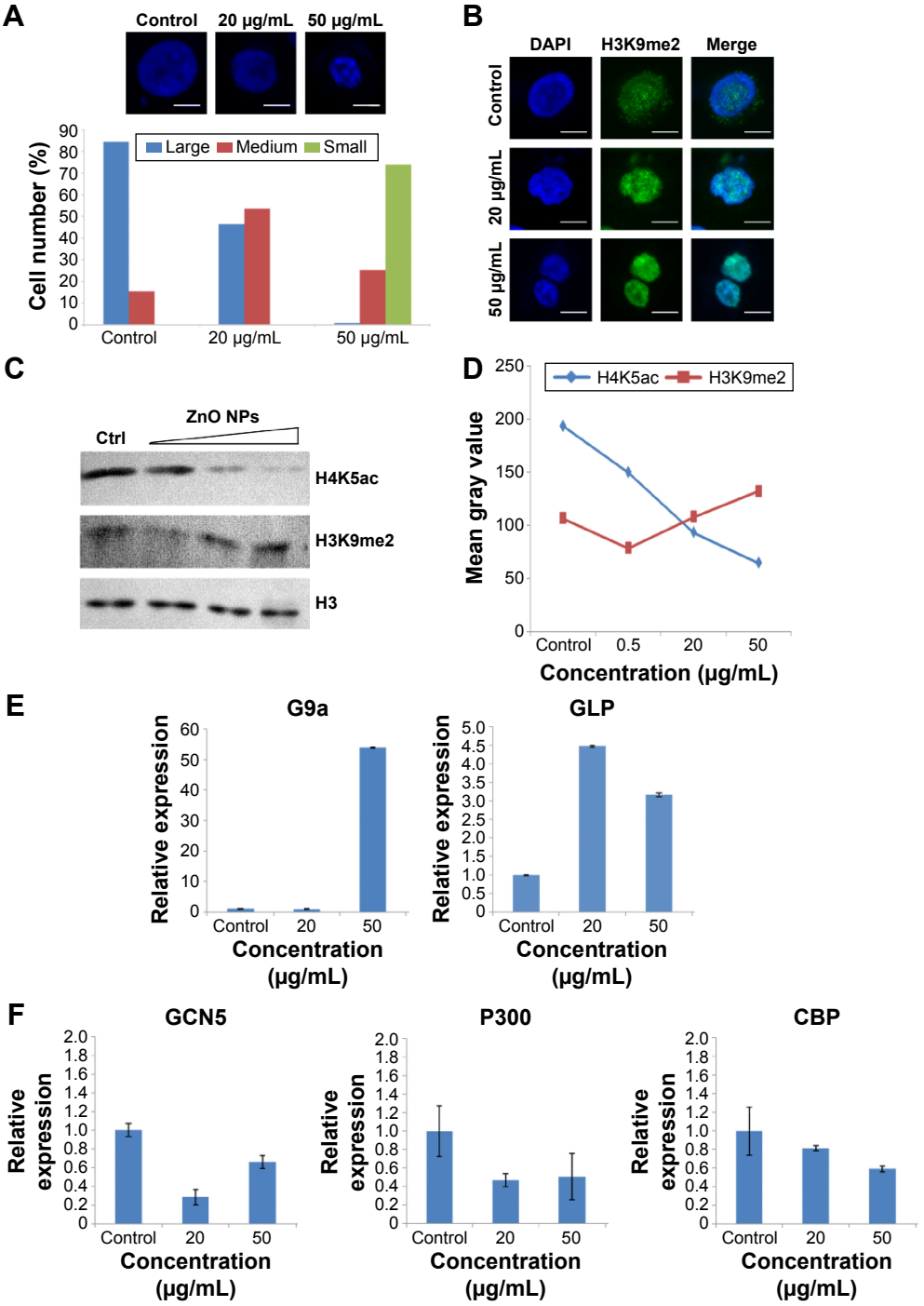

Figure 3 The alterations of chromatin modifications and the expression of histone methyltransferase genes and acetyltransferase genes in HaCaT cells after exposure to ZnO NPs.

Notes: (**A**) Nuclear changes induced by ZnO NPs were detected by a fluorescence microscope. HaCaT cells were grown on glass coverslips, untreated (control) or treated for 24 hours with ZnO NPs (20 or 50 μg/mL) and stained with DAPI (blue). Scale bars =10 μm. Percentages of the nucleus in different sizes (large, medium, small) after 24-hour exposure to ZnO NPs at 20 and 50 μg/mL. Number of evaluated cells in each group was 300. (**B**) The histone H3K9 in nucleus in HaCaT cells undergoes increased methylation after ZnO NPs treatment. HaCaT cells were grown on glass coverslips, untreated (control) or treated for 24 hours with ZnO NPs (20 or 50 μg/mL) and stained with DAPI (blue). The same cells were also stained with the H3K9me2 antibody, followed by anti-rabbit secondary antibody (green). Scale bars =10 μm. (**C**) A decrease in global H4K5ac and an increase in global H3K9me2 were observed after treatment with 0.5, 20, and 50 μg/mL ZnO NPs compared with the control group. Histone H3 was used as a protein loading control. (**D**) Histogram showing the mean gray values of the Western blot bands for histone modifications. The experiments were repeated three times using biologically independent samples. (**E**) ZnO NPs induced the increased expression of methyltransferase genes *G9a* and *GLP*; the expression of both G9a and GLP genes was increased at 50 μg/mL, whereas the expression of only GLP gene was increased at 20 μg/mL. (**F**) The expression of acetyltransferase genes *GCN5*, *P300*, and *CBP* was decreased compared to control. The relative expression value of the control group (untreated) was defined as 1.0. The actin gene was used as an internal control. The data are represented as the mean ± standard error for triplicate quantitative PCRs for each concentration from three independent experiments.

Abbreviations: ZnO NPs, zinc oxide nanoparticles; DAPI, 4,6-diamidino-2-phenylindole; PCR, polymerase chain reaction.

20 or 50 μg/mL ZnO NPs. After treatment with 50 μg/mL ZnO NPs, the mRNA level was nearly 50-fold higher for the methyltransferase gene *G9a* than in control cells and nearly fivefold higher for the *GLP* gene (Figure 3E). By contrast, the expression of acetyltransferase genes *GCN5*, *P300*, and *CBP* decreased significantly after treatment with ZnO NPs (Figure 3F). The change in expression of these epigenetic enzyme genes might contribute to the alteration of the chromatin modification levels, suggesting that chromatin structure changes mediated by epigenetic modification were involved in the cell cycle arrest.

ZnO NPs induced production of ROS and DNA damage in HaCaT cells

NPs have been reported to be able to induce oxidative stress within cells, which often results in DNA damage.[12,13,32] Therefore, ROS formation and DNA damage in treated HaCaT cells were analyzed to investigate their possible involvement in the induction of G2/M arrest. The data presented here showed that the ROS content increased after treatment with 20 μg/mL ZnO NPs for 6 hours (Figure 4B) compared with the control (Figure 4A), and then it fell to the control level after 24 hours and remained so until the tenth day (Figure 4C and D). DNA damage induced cell cycle arrest in the G2/M phase, and the G2/M checkpoint prevented DNA-damaged cells from entering mitosis to allow for the repair of DNA prior to mitosis.[33,34] The phosphorylation of the core histone variant H2AX (γ-H2AX), the best marker of DNA damage-induced histone modification,[35] serves as a hallmark of DNA double-strand breaks.[36,37] Therefore, we measured the distributions of γ-H2AX in the nucleus after exposure to ZnO NPs for 24 hours (Figure 5A). The immunostaining results showed that the γ-H2AX signals were increased significantly in treated samples compared with controls, and the signals after 20 μg/mL treatment were dispersed throughout the whole nucleus, whereas the signals after 50 μg/mL treatment were stronger (Figure 5A). Western blot showed increased γ-H2AX signals after treatment with 20 or 50 μg/mL ZnO NPs compared with the control group, and there was more damage after treatment with 50 μg/mL ZnO NPs than with 20 μg/mL (Figure 5B). The accumulation of γ-H2AX signals indicated that DNA breaks had occurred and that the damage exacerbated with higher concentrations of ZnO NPs, consistent with the report of Toduka et al, who observed increased γ-H2AX signals in cultured (CHO)-K1 cells after exposure to increasing concentrations of ZnO NPs.[38]

ZnO NPs are absorbed into HaCaT cells

Because NPs appear to exert different cytotoxicities, depending on the cellular uptake, localization, and translocation,[21,39] we assessed NP uptake and localization in HaCaT cells using TEM and flow cytometry. TEM images showed that no ZnO NPs were found in the cytoplasm and nucleus of the control cells (Figure 6A-a and A-e), but ZnO NPs were detected as aggregates dispersed inside the cytoplasm instead of as single particles after treatment with 20 μg/mL ZnO NPs (Figure 6A-b and A-f). Surprisingly, after exposure to ZnO NPs at 50 μg/mL for 24 hours, the aggregates were found to have accumulated in the perinuclear region (Figure 6A-c and A-g). We also found that the membrane of mitochondria was squeezed by ZnO NPs (Figure 6A-d and A-h) after treatment with 50 μg/mL ZnO NPs for 24 hours. Flow cytometric uptake analysis showed that the nanomaterial affected the SSC, which is related to nanomaterial uptake or changes in the organelles within the cell (Figure 6B). We found that the SSC of cells showed a large increase due to the uptake of a substantial amount of ZnO NPs, and control cells showed a size distribution population with minimal SSC. These results suggested that ZnO NPs were capable of entering the cell and interacting with mitochondria and nuclei, therefore resulting in mitochondrial damage and chromatin changes.

ZnO NPs induced HaCaT cell apoptosis

It has been reported that NPs can induce cell apoptosis.[21] More specifically, if the damage is irreparable, checkpoint signaling might activate pathways that lead to apoptosis.[31,33,40] The finding that ZnO NPs induced cell cycle arrest and DNA repair in treated HaCaT cells prompted us to examine whether apoptosis occurred in these treated cells. The SEM images showed that the untreated control cells remained smooth and flat with a cell surface covered by microvillar structures that were well extended with small lamellapodia (Figure 7A), indicating the fluidity and motility of normal cells. However, the surface of HaCaT cells did not have obvious microvilli, and some membrane blebs (Figure 7A, arrows) were clearly observed in HaCaT cells treated with 20 and 50 μg/mL ZnO NPs. The blebbing of the plasma membrane into smaller membrane-bound apoptotic bodies is a common structural feature of apoptotic cells.[41–43] To further confirm apoptosis induced by ZnO NPs, we used Annexin-V-FITC and PI assays to count the ratio of apoptotic cells (Figure 7B). After exposure to ZnO NPs for 24 hours, the numbers of apoptotic cells increased markedly. Furthermore, as the exposure concentration increased from 20 to 50 μg/mL, the total number of apoptotic cells increased from 14.54% to 43.13%.

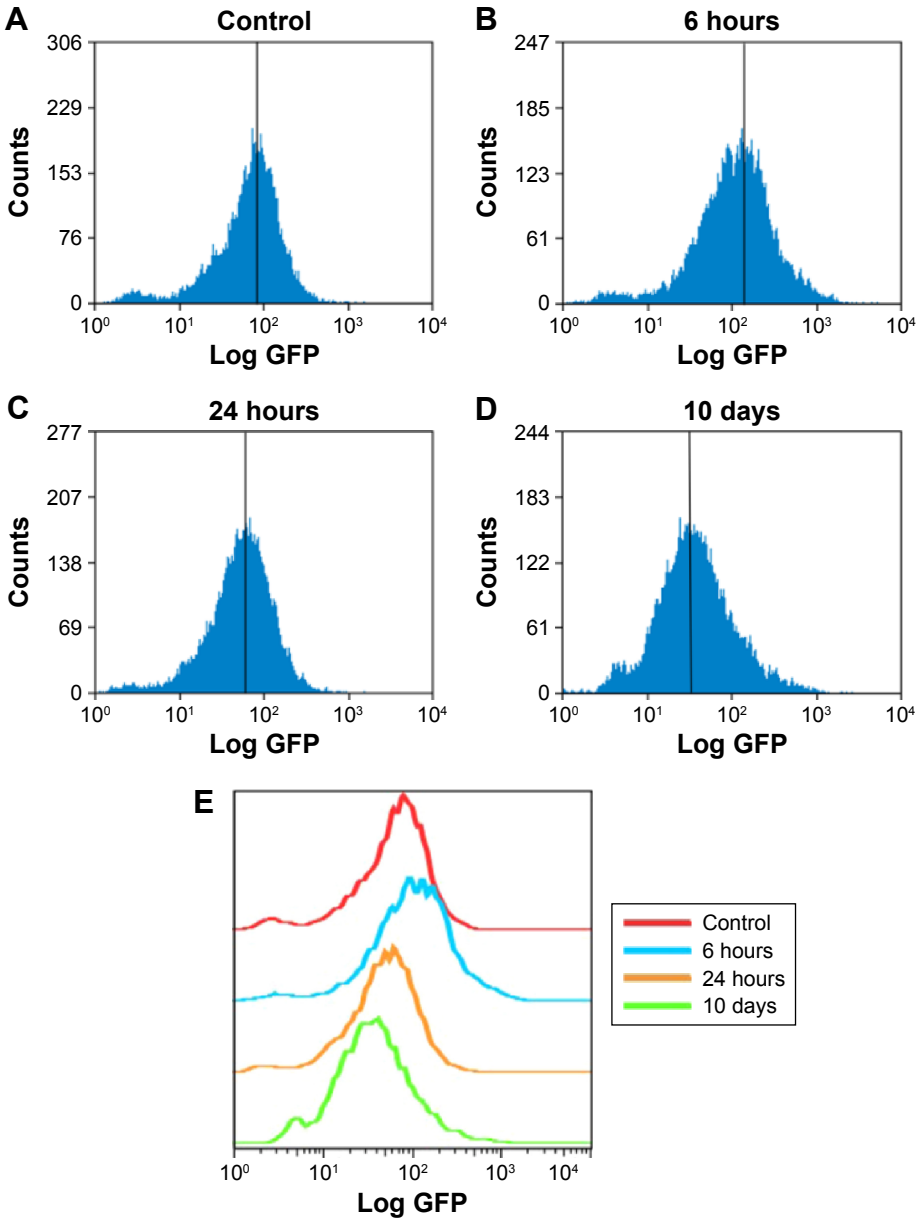

Figure 4 ZnO NPs induced the production of ROS in HaCaT cells.
Notes: Cells grown in a culture plate were treated with nanoparticles at 20 μg/mL for (**A**) 0, (**B**) 6, or (**C**) 24 hours, or (**D**) 10 days, washed with cold phosphate-buffered saline, and then incubated with DCFH-DA. The samples were measured by flow cytometry. (**E**) Relative analysis of each sample by software FlowJo 7.6. The *x*-axis shows the intensity of fluorescence representing the level of ROS, and the *y*-axis shows the measured cell quantity.
Abbreviations: ROS, reactive oxygen species; DCFH-DA, 2′,7′-dichlorodihydrofluorescein diacetate.

These results suggested that ZnO NPs can induce HaCaT cell apoptosis that was characterized by morphological changes on the cell membrane.

Expression of apoptosis-related genes was upregulated in HaCaT cells after exposure to ZnO NPs

To understand the molecular mechanism of apoptosis induced by ZnO NPs, we measured the expression of several genes involved in triggering or preventing apoptosis (Figure 8). The results showed that expression of the proapoptotic genes *Bax*, *Noxa*, and *Puma* increased nearly tenfold, 15-fold, and 300-fold, respectively, after treatment with 50 μg/mL ZnO NPs. The mRNA level of the *Bax* gene was nearly fourfold higher, whereas the mRNA level of the *Noxa* and *Puma* genes was unchanged after 20 μg/mL treatment. The expression of the gene *Bcl-xl*, an inhibitor of apoptosis involved in preventing cell death, was reduced, whereas the mRNA expression of the *Bcl-2* (inhibitor of apoptosis) gene was increased and that of the *Hsp70* was unchanged. The data presented here

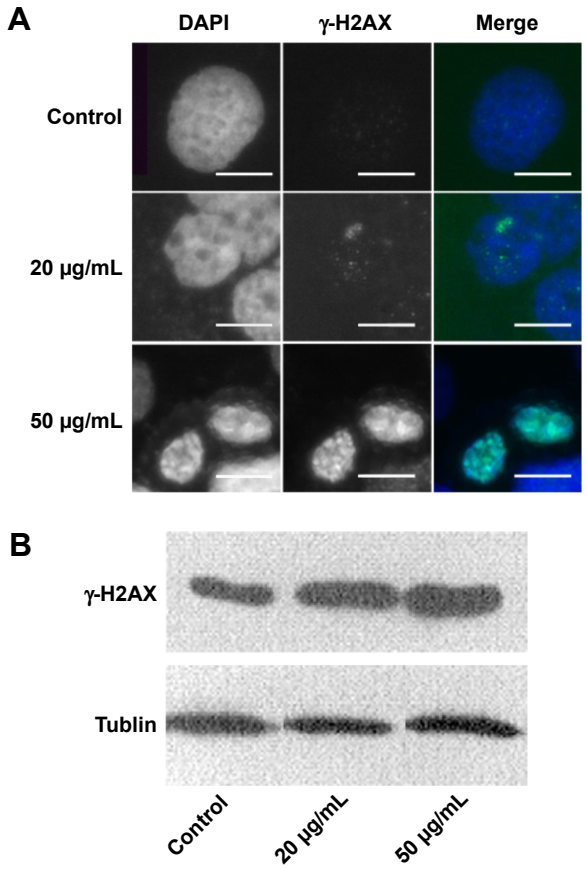

Figure 5 The nucleus in HaCaT cells showed increased γ-H2AX signals after ZnO NPs treatment.
Notes: (**A**) HaCaT cells were grown on glass coverslips, untreated (control) or treated (20 or 50 μg/mL) for 24 hours with ZnO NPs and stained with DAPI (blue). The same cells were also stained with the γ-H2AX antibody, followed by the anti-rabbit secondary antibody (green). Scale bars =10 μm. (**B**) An increase in γ-H2AX signals was observed after treatment with 20 and 50 μg/mL ZnO NPs compared with the control group. Tublin was used as a protein-loading control.
Abbreviations: ZnO NPs, zinc oxide nanoparticles; DAPI, 4,6-diamidino-2-phenylindole.

indicated that *Bax*, *Noxa*, and *Puma* might be involved in the induction of apoptosis by upregulation within the cell. The expression of the antiapoptotic gene *Bcl-2* was activated in the proapoptotic state, but the function of *Bcl-2* may be prevented by *Puma*, which contributes indirectly to the regulation of the *Bcl-2* family members *Bax* and/or *Bak* by relieving the inhibition imposed by antiapoptotic members. The expression of Bcl family genes relevant to the mitochondrial apoptotic pathway indicated that the apoptosis induced by ZnO NPs may involve mitochondrial damage.[44,45]

Discussion

The rapid growth of nanotechnology has had a significant impact on the quality of human life. Both the design of functionalized NPs and the application of NP-based medicines demand an understanding of the behavior and effects of NPs in living systems. The specific epigenomic response would provide new insights into genetic regulation and its role in cellular growth, differentiation, cell death, diseases, and aging.[18] Some studies on the evaluation of the cyto- and genosafety of ZnO NPs have been reported,[6,9,46–50] but only few have focused on an epigenomic safety evaluation, even when cyto- and genotoxicity is not apparent. In this study, we examined the effects of ZnO NPs on HaCaT cells as a model for exposed skin at the epigenomic level as well as at the cellular and molecular levels. The results showed that 100 nm ZnO NPs could alter normal cell cycle progression, causing a G2/M arrest that proceeds the loss of viability of HaCaT cells, that was associated with epigenetic changes and accompanied by p53-Bax mitochondrial pathway-mediated apoptosis (Figure 9).

ZnO NP exposure has previously been reported to result in cellular changes at various phases of the cell cycle.[11,14,15] The characteristics of ZnO NPs, the dose, the treatment time, and the specific cell line selected may affect the results obtained.[48,51] The data presented here showed that the cell cycle was arrested at the G2/M phase after treatment with 50 μg/mL of 100 nm ZnO NPs for 24 hours (Figure 2C), suggesting that the HaCaT cells exposed to ZnO NPs were unable to go through mitosis, leading to the subsequent decreased cell viability at 48 hours.

Cell cycle arrest is often linked to the DNA damage response and involves changes in histone modification.[30,31,34] DNA damage-induced cell cycle arrest at the G2/M phase and the G2/M checkpoint would prevent DNA-damaged cells from entering mitosis to allow for the repair of DNA prior to mitosis.[31,33,40,52] Previous evidence suggested that the global chromatin structure is remodeled in response to external cues.[35,53,54] Additionally, DNA damage-induced histone modifications and/or preexisting modified histones in the vicinity of the broken chromatin may provide docking sites for DNA damage response proteins.[55–57] Our results showed that H4K5ac levels decreased fourfold with increasing ZnO NP concentrations; by contrast, H3K9me2 signals increased nearly 1.5-fold (Figure 3C and D). The increase in methylated residues in histone H3 and the decrease in acetylated residues in histone H4 near the break regions might provide signals for the recruitment of DNA repair proteins, including chromatin remodeling complexes. The accumulation of γ-H2AX signals indicated that DNA breaks occurred, possibly resulting in remodeling of the chromatin structure, for example, chromatin condensation and nucleus shrinking.

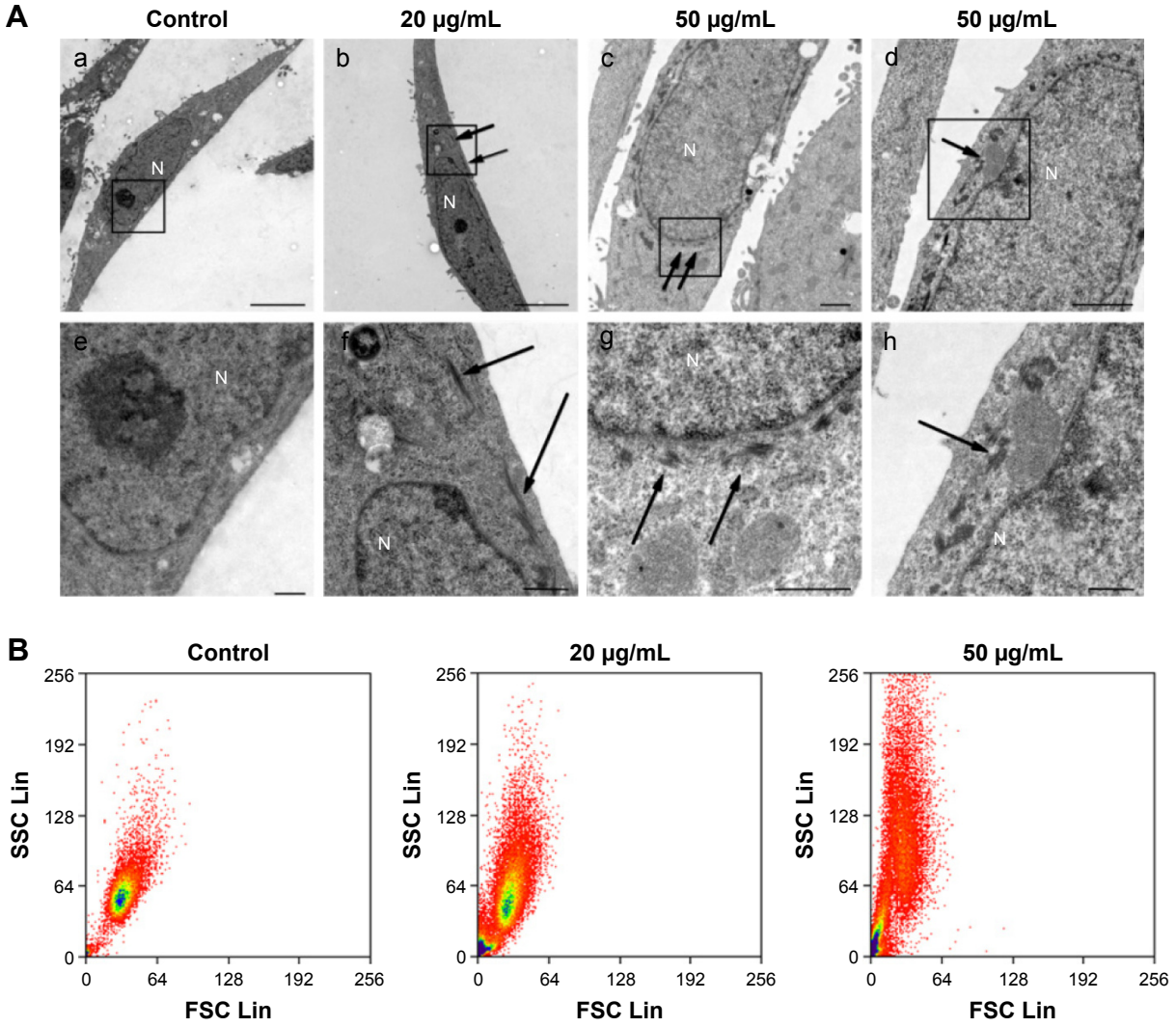

Figure 6 Analysis of nanomaterial uptake by cells.

Notes: (**A**) TEM images of HaCaT cells treated with ZnO NPs at 20 and 50 μg/mL for 24 hours: (a) No ZnO NP was observed in the control cytoplasm and nucleus. (b) The aggregates of ZnO NPs were observed dispersedly in the cytoplasm (arrows), but not in the nucleus, after cells were treated with ZnO NPs for 24 hours. (c) The nucleus was surrounded by the aggregates of ZnO NPs (arrows), but no ZnO NP was observed in the other area of the cell. (d) The membrane of mitochondria was squeezed by ZnO NPs (arrows). Images e–h are the high-magnification images of the black boxed regions of images a–d. Scale bars: 5 μm in a and b, 1 μm in c and d, and 500 nm in e–h. (**B**) Flow cytometry analysis of nanoparticle uptake in HaCaT cells exposed to ZnO NPs for 24 hours. The SSC intensity representing granularity of a cell and the FSC representing the size of a cell were analyzed with flow cytometry. Nanomaterial uptake/surface adsorption is reflected by an increase in the SSC of cell populations.

Abbreviations: TEM, transmission electron microscopy; ZnO NPs, zinc oxide nanoparticles; SSC, side scatter; FSC, forward scatter; N, nucleus.

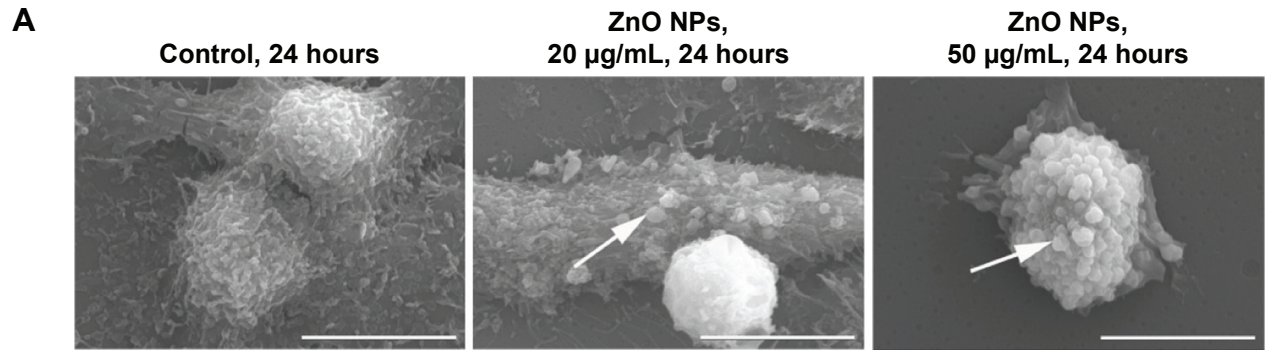

Figure 7 (*Continued*)

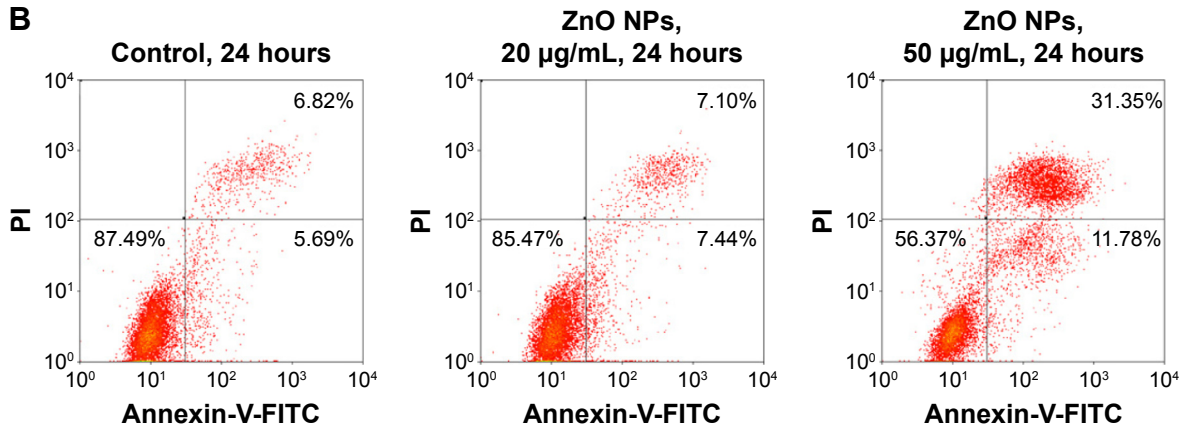

Figure 7 ZnO NPs induced HaCaT cell apoptosis.

Notes: (**A**) Scanning electron microscopy images of HaCaT cell topography after exposure to ZnO NPs for 24 hours at different concentrations. The normal HaCaT surface was covered by abundant microvillus, whereas after exposure to ZnO NPs, the microvillus was decreased significantly. Compared to normal HaCaT cells, the apoptotic body appeared (white arrows) on the surface of treated cells. Scale bars =10 μm. (**B**) Flow cytometry results of Annexin-V-FITC and PI assay. HaCaT cells were treated without (control) or with ZnO NPs (20 or 50 μg/mL) for 24 hours. A cell stained by Annexin-V-FITC$^-$ and PI$^-$ is shown in the lower left area, one stained by Annexin-V-FITC$^+$ and PI$^-$ is shown in the lower right area, one stained by Annexin-V-FITC$^-$ and PI$^+$ is shown in the upper left area, and one stained by Annexin-V-FITC$^+$ and PI$^+$ is shown in the upper right area.

Abbreviations: ZnO NPs, zinc oxide nanoparticles; FITC, fluorescein isothiocyanate; PI, propidium iodide.

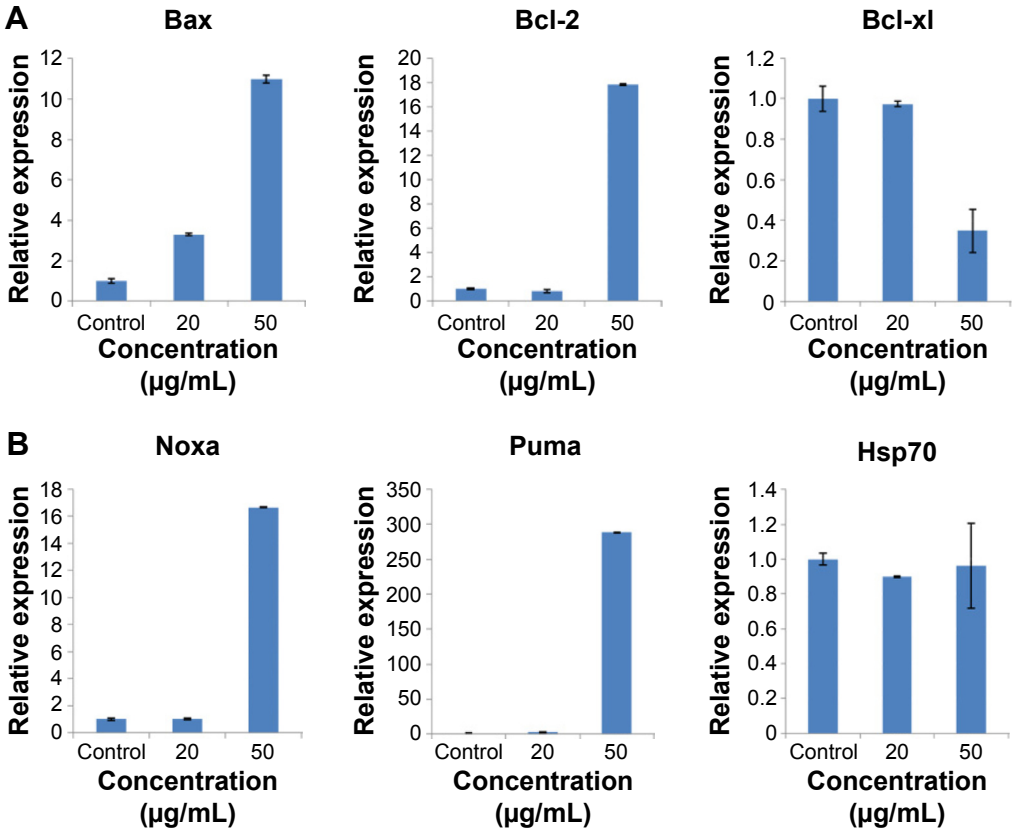

Figure 8 The expression of apoptotic relevant genes in HaCaT cells after exposure to ZnO NPs for 24 hours measured by real-time PCR.

Notes: (**A**) Mitochondrial apoptotic pathway-relevant Bcl family genes. ZnO NPs induced the increased expression of proapoptotic gene Bax and antiapoptotic gene Bcl-2 and induced the decreased expression of antiapoptotic gene Bcl-xl. (**B**) The expression of apoptotic genes Noxa and Puma was increased, and that of Hsp70 was unaffected. The relative expression value of the control group (untreated) was defined as 1.0. The actin gene was used as an internal control. The data are represented as the mean ± standard error for triplicate quantitative PCRs for each concentration from three independent experiments.

Abbreviations: ZnO NPs, zinc oxide nanoparticles; PCR, polymerase chain reaction.

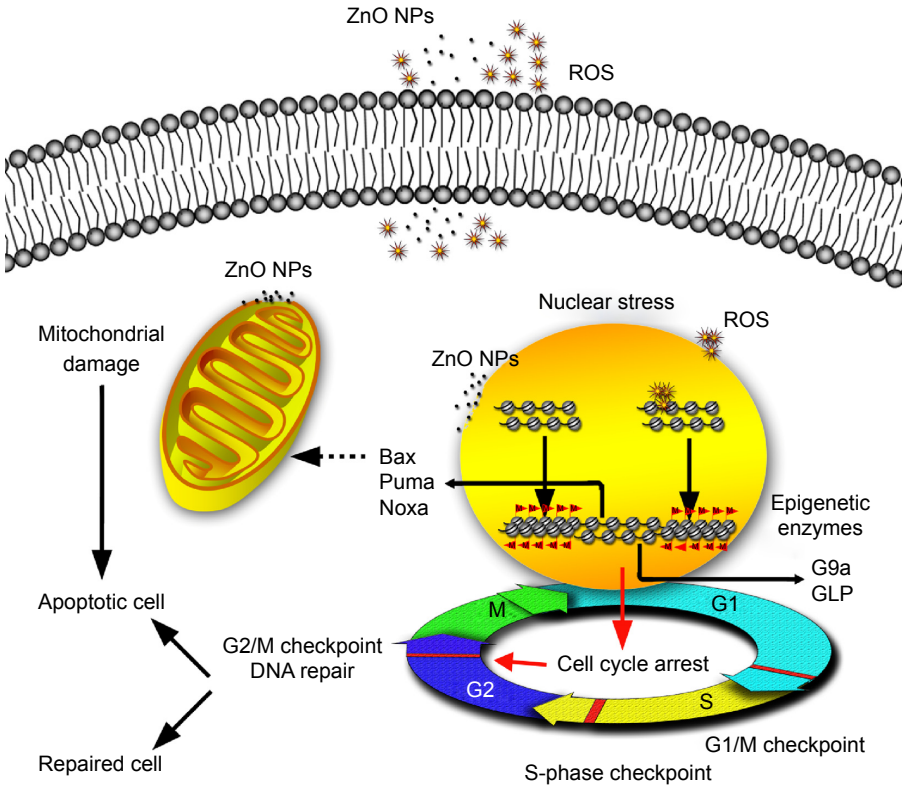

Figure 9 Possible mechanisms involved in ZnO NP-induced changes in HaCaT cells at epigenetic and molecular levels.
Notes: ZnO NPs release ROS extra- and intracellularly. The transient ROS explosion and the ZnO NPs accumulated in perinucleus might result in G2/M cell cycle arrest associated with the nuclear stress (DNA damage and chromatin structure remodeling) before the viability of HaCaT cells was reduced. When the nucleus is subjected to stress, histone lysine residue modifications (H4K5ac and H3K9me2) near the DNA break regions might provide signals for recruitment of DNA repair proteins, resulting in the chromatin structure remodeling such as chromatin condensation and nucleus shrinking. The G2/M checkpoint prevented DNA-damaged cells from entering mitosis to allow for the repair of DNA prior to mitosis; the checkpoint signaling might activate pathways that lead to apoptosis if the damage is irreparable. The upregulation of the proapoptotic Bcl-2 family relevant genes Bax, Noxa, and Puma that are related to mitochondrial apoptotic pathway indicates that the apoptosis induced by ZnO NPs may be involved in mitochondrion damage. The mitochondrion squeezed by ZnO NPs directly may also result in mitochondrion dysfunction and subsequent cell apoptosis.
Abbreviations: ZnO NPs, zinc oxide nanoparticles; ROS, reactive oxygen species.

G9a and GLP are the major homologous mammalian histone methyltransferases that methylate histone H3 at Lys9[58] and cooperatively rather than redundantly mediate H3K9 mono- and di-methylation at euchromatin regions.[59] G9a transfers methyl groups to the lysine residues of histone H3, with ten- to 20-fold higher activity than other histone methyltransferases,[58] such as Suv39 h1, which contributes to methylation on pericentric heterochromatin.[59] The mRNA level increased nearly 50-fold for the methyltransferase gene *G9a* and nearly fivefold for the methyltransferase gene *GLP* after exposure to 50 μg/mL ZnO NPs, which suggested that the lysine-terminal tails in histone H3 might be selectively methylated by methyltransferases G9a and GLP, and G9a might play a major role in this methylation state. With increased methylation by G9a and GLP at euchromatin regions, the euchromatin was likely to be transformed into heterochromatin because increased methylation of histone H3 throughout heterochromatin regions was detected (Figure 3B). This ZnO NP-induced hypermethylation of chromatin might control the accessibility of damaged regions of DNA to repair signaling proteins.[55,56]

The ability of NPs to induce toxicity has been attributed to their increased surface reactivity.[60,61] Smaller particles have a higher surface area per unit mass, resulting in production of more ROS in the cellular environment.[62,63] ROS generated by NPs can deplete endogenous antioxidants, alter mitochondrial function, and cause oxidative damage to DNA.[63] In our study, the ROS content increased after treatment with 20 μg/mL ZnO NPs for 6 hours (Figure 4B), suggesting that the ROS explosion was an early event in response to ZnO NP-mediated stress and occurred before the viability of HaCaT cells decreased. The explosive ROS subsequently caused DNA damage accompanied by histone modification change, which resulted in cell cycle arrest. Our results also showed that the ROS content fell to control levels after 24 hours (Figure 4C and D), suggesting that ROS content might be

eliminated by endogenous antioxidants, but the induced DNA damage still disturbed the cell cycle.

The particle size, particle morphology, functional groups on the NP surface, and the cell type determined the subcellular distribution of NPs and then resulted in variable toxicity and subsequent cell fate.[21] Albini et al reported that single-walled carbon nanotubes (SWCNTs) were taken up into acidic vesicles within the endothelial cells, using the neutral red uptake assay, the LysoTracker lysosome test, and dispersive Raman "imaging".[64] Yaron et al reported that 145 nm-long SWCNTs were located in the perinuclear region of HeLa cells, observed by confocal Raman spectroscopy, suggesting that SWCNTs entered cells via endocytosis, disrupted some of the endosomes as they shrank into lysosomes, and were then deposited in or near the endoplasmic reticulum.[65] De Berardis et al reported that nuclei with condensed and marginalized chromatin and mitochondria with shrunken, condensed matrices, and swollen cristae were induced by 50–70 nm ZnO NPs in human colon carcinoma cells.[66] Our results showed that 100 nm ZnO NP aggregates accumulated in the perinucleus (Figure 6A-c and A-g), accompanied by chromatin condensation. The aggregates accumulated in the perinucleus might interact with the nucleus directly or indirectly.[13] Previous research showed that nuclear membranes, nuclear laminae, and nucleolar functions were compromised by small spherical Au NPs or gold nanoflowers in breast cancer cells.[67] Dam et al reported that nanoconstructs composed of nucleolin-specific aptamers and gold nanostars were transferred to the perinuclear region and induced major changes to the nuclear phenotype via nuclear envelope invaginations.[68] Therefore, the nucleus might be mechanically disturbed by ZnO NP aggregates located in the perinucleus or by the ROS induced by these aggregates. The cell nucleus functions to maintain all processes that occur within the cell, and any disruptions within the nucleus would subsequently affect the cellular chromatin, thereby disturbing the highly regulated cell cycle.[69] We also observed that the membrane of mitochondria was squeezed by ZnO NPs (Figure 6A-d and A-h), suggesting that the mitochondria could be mechanically disturbed by ZnO NPs.

The G2/M checkpoint prevents cells from entering mitosis when DNA is damaged to provide these cells an opportunity to repair the damaged DNA before propagating the genetic defects to daughter cells. If the damage is irreparable, checkpoint signaling might activate pathways that lead to apoptosis.[40] Our results showed that the cell cycle was arrested at the G2/M phase, in agreement with the result reported in the literature,[40] and cell apoptosis subsequently occurred. The tumor suppressor protein p53-related pathway is involved in DNA repair and the apoptotic response to maintain genomic stability.[44] The proapoptotic protein Bax is a requisite gateway to mitochondrial dysfunction and death.[45] To explore the mechanism of apoptosis associated with G2/M cell cycle arrest, we examined the expression of relevant apoptotic genes. The increased expression of the proapoptotic genes *Bax*, *Noxa*, and *Puma* and the decreased expression of the antiapoptotic gene *Bcl-xl* suggested that the *Bcl-2* family might be involved in the apoptosis through mitochondrial dysfunction.

Conclusion

This study provides new insights into genetic regulation and its role in cellular growth and death after exposure to ZnO NPs, offers an epigenomic safety evaluation even when cyto- and genotoxicity are not apparent, and gives support to the future use of ZnO NPs for cellular therapeutic applications. Further investigations into the long-term effects of NPs on epigenetic modifications and subsequent recovery assays after NP exposure will be required.

Acknowledgments

The authors thank Dr Shihan Yan for excellent technical assistance. This work was supported by the National Natural Science Foundation of China (number 31571265).

Disclosure

The authors report no conflicts of interest in this work.

References

1. Brayner R. The toxicological impact of nanoparticles. *Nano Today*. 2008;3(1):48–55.
2. Nel A, Xia T, Meng H, et al. Nanomaterial toxicity testing in the 21st century: use of a predictive toxicological approach and high-throughput screening. *Acc Chem Res*. 2012;46(3):607–621.
3. Nohynek G, Dufour E, Roberts M. Nanotechnology, cosmetics and the skin: is there a health risk? *Skin Pharmacol Physiol*. 2008;21(3):136–149.
4. Nohynek GJ, Lademann J, Ribaud C, Roberts MS. Grey goo on the skin? Nanotechnology, cosmetic and sunscreen safety. *Crit Rev Toxicol*. 2007;37(3):251–277.
5. Kim CS, Nguyen HD, Ignacio RM, et al. Immunotoxicity of zinc oxide nanoparticles with different size and electrostatic charge. *Int J Nanomedicine*. 2014;9 Suppl 2:195–205.
6. Adamcakova-Dodd A, Stebounova LV, Kim JS, et al. Toxicity assessment of zinc oxide nanoparticles using sub-acute and sub-chronic murine inhalation models. *Part Fibre Toxicol*. 2014;11:15.
7. Alarifi S, Ali D, Alkahtani S, et al. Induction of oxidative stress, DNA damage, and apoptosis in a malignant human skin melanoma cell line after exposure to zinc oxide nanoparticles. *Int J Nanomedicine*. 2013;8:983–993.
8. Kumar A, Najafzadeh M, Jacob BK, Dhawan A, Anderson D. Zinc oxide nanoparticles affect the expression of p53, Ras p21 and JNKs: an ex vivo/in vitro exposure study in respiratory disease patients. *Mutagenesis*. 2015;30(2):237–245.

9. Premanathan M, Karthikeyan K, Jeyasubramanian K, Manivannan G. Selective toxicity of ZnO nanoparticles toward Gram-positive bacteria and cancer cells by apoptosis through lipid peroxidation. *Nanomedicine*. 2011;7(2):184–192.
10. Akhtar MJ, Ahamed M, Kumar S, Khan MM, Ahmad J, Alrokayan SA. Zinc oxide nanoparticles selectively induce apoptosis in human cancer cells through reactive oxygen species. *Int J Nanomedicine*. 2012; 7:845–857.
11. Kocbek P, Teskač K, Kreft ME, Kristl J. Toxicological aspects of long-term treatment of keratinocytes with ZnO and TiO2 nanoparticles. *Small*. 2010;6(17):1908–1917.
12. Sharma V, Anderson D, Dhawan A. Zinc oxide nanoparticles induce oxidative DNA damage and ROS-triggered mitochondria mediated apoptosis in human liver cells (HepG2). *Apoptosis*. 2012;17(8):852–870.
13. Sharma V, Shukla RK, Saxena N, Parmar D, Das M, Dhawan A. DNA damaging potential of zinc oxide nanoparticles in human epidermal cells. *Toxicol Lett*. 2009;185(3):211–218.
14. Mahmoudi M, Azadmanesh K, Shokrgozar MA, Journeay WS, Laurent S. Effect of nanoparticles on the cell life cycle. *Chem Rev*. 2011; 111(5):3407–3432.
15. Valdiglesias V, Costa C, Kiliç G, et al. Neuronal cytotoxicity and genotoxicity induced by zinc oxide nanoparticles. *Environ Int*. 2013; 55:92–100.
16. Farnebo M, Bykov VJ, Wiman KG. The p53 tumor suppressor: a master regulator of diverse cellular processes and therapeutic target in cancer. *Biochem Biophys Res Commun*. 2010;396(1):85–89.
17. Strahl BD, Allis CD. The language of covalent histone modifications. *Nature*. 2000;403(6765):41–45.
18. Callinan PA, Feinberg AP. The emerging science of epigenomics. *Hum Mol Genet*. 2006;15(Suppl 1):R95–R101.
19. Esteller M. The necessity of a human epigenome project. *Carcinogenesis*. 2006;27(6):1121–1125.
20. Pan Y, Wang L, Kang S-G, et al. Gd–metallofullerenol nanomaterial suppresses pancreatic cancer metastasis by inhibiting the interaction of histone deacetylase 1 and metastasis-associated protein 1. *ACS Nano*. 2015;9(7):6826–6836.
21. Sohaebuddin SK, Thevenot PT, Baker D, Eaton JW, Tang L. Nanomaterial cytotoxicity is composition, size, and cell type dependent. *Part Fibre Toxicol*. 2010;7(1):22.
22. Kodiha M, Wang YM, Hutter E, Maysinger D, Stochaj U. Off to the organelles-killing cancer cells with targeted gold nanoparticles. *Theranostics*. 2015;5(4):357.
23. Huo S, Jin S, Ma X, et al. Ultrasmall gold nanoparticles as carriers for nucleus-based gene therapy due to size-dependent nuclear entry. *ACS Nano*. 2014;8(6):5852–5862.
24. Rasmussen JW, Martinez E, Louka P, Wingett DG. Zinc oxide nanoparticles for selective destruction of tumor cells and potential for drug delivery applications. *Expert Opin Drug Deliv*. 2010;7(9):1063–1077.
25. Boukamp P, Popp S, Altmeyer S, et al. Sustained nontumorigenic phenotype correlates with a largely stable chromosome content during long-term culture of the human keratinocyte line HaCaT. *Genes Chromosomes Cancer*. 1997;19(4):201–214.
26. Yang X, Liu J, He H, et al. SiO2 nanoparticles induce cytotoxicity and protein expression alteration in HaCaT cells. *Part Fibre Toxicol*. 2010;7(1):1.
27. Gius DR, Ezhevsky SA, Becker-Hapak M, Nagahara H, Wei MC, Dowdy SF. Transduced p16INK4a peptides inhibit hypophosphorylation of the retinoblastoma protein and cell cycle progression prior to activation of Cdk2 complexes in late G1. *Cancer Res*. 1999;59(11): 2577–2580.
28. Suzuki H, Toyooka T, Ibuki Y. Simple and easy method to evaluate uptake potential of nanoparticles in mammalian cells using a flow cytometric light scatter analysis. *Environ Sci Technol*. 2007;41(8): 3018–3024.
29. Nieswandt B, Bergmeier W, Schulte V, Rackebrandt K, Gessner JE, Zirngibl H. Expression and function of the mouse collagen receptor glycoprotein VI is strictly dependent on its association with the FcRγ chain. *J Biol Chem*. 2000;275(31):23998–24002.
30. Osley M. The regulation of histone synthesis in the cell cycle. *Annu Rev Biochem*. 1991;60(1):827–861.
31. Rieder CL. Mitosis in vertebrates: the G2/M and M/A transitions and their associated checkpoints. *Chromosome Res*. 2011;19(3): 291–306.
32. Sharma V, Singh P, Pandey AK, Dhawan A. Induction of oxidative stress, DNA damage and apoptosis in mouse liver after sub-acute oral exposure to zinc oxide nanoparticles. *Mutat Res*. 2012;745(1):84–91.
33. Rich T, Allen RL, Wyllie AH. Defying death after DNA damage. *Nature*. 2000;407(6805):777–783.
34. Groth A, Rocha W, Verreault A, Almouzni G. Chromatin challenges during DNA replication and repair. *Cell*. 2007;128(4):721–733.
35. Kruhlak MJ, Celeste A, Dellaire G, et al. Changes in chromatin structure and mobility in living cells at sites of DNA double-strand breaks. *J Cell Biol*. 2006;172(6):823–834.
36. Rogakou EP, Pilch DR, Orr AH, Ivanova VS, Bonner WM. DNA double-stranded breaks induce histone H2AX phosphorylation on serine 139. *J Biol Chem*. 1998;273(10):5858–5868.
37. Fernandez-Capetillo O, Allis CD, Nussenzweig A. Phosphorylation of histone H2B at DNA double-strand breaks. *J Exp Med*. 2004;199(12): 1671–1677.
38. Toduka Y, Toyooka T, Ibuki Y. Flow cytometric evaluation of nanoparticles using side-scattered light and reactive oxygen species-mediated fluorescence–correlation with genotoxicity. *Environ Sci Technol*. 2012;46(14):7629–7636.
39. Zhao F, Zhao Y, Liu Y, Chang X, Chen C, Zhao Y. Cellular uptake, intracellular trafficking, and cytotoxicity of nanomaterials. *Small*. 2011;7(10):1322–1337.
40. Pearce AK, Humphrey TC. Integrating stress-response and cell-cycle checkpoint pathways. *Trends Cell Biol*. 2001;11(10):426–433.
41. Casciola-Rosen LA, Anhalt G, Rosen A. Autoantigens targeted in systemic lupus erythematosus are clustered in two populations of surface structures on apoptotic keratinocytes. *J Exp Med*. 1994;179(4): 1317–1330.
42. Häcker G. The morphology of apoptosis. *Cell Tissue Res*. 2000; 301(1):5–17.
43. Taylor RC, Cullen SP, Martin SJ. Apoptosis: controlled demolition at the cellular level. *Nat Rev Mol Cell Biol*. 2008;9(3):231–241.
44. McCurrach ME, Connor TM, Knudson CM, Korsmeyer SJ, Lowe SW. Bax-deficiency promotes drug resistance and oncogenic transformation by attenuating p53-dependent apoptosis. *Proc Natl Acad Sci U S A*. 1997;94(6):2345–2349.
45. Wei MC, Zong W-X, Cheng EH-Y, et al. Proapoptotic BAX and BAK: a requisite gateway to mitochondrial dysfunction and death. *Science*. 2001;292(5517):727–730.
46. Huang K-L, Lee Y-H, Chen H-I, Liao H-S, Chiang B-L, Cheng T-J. Zinc oxide nanoparticles induce eosinophilic airway inflammation in mice. *J Hazard Mater*. 2015;297:304–312.
47. Cho W-S, Duffin R, Howie S, et al. Progressive severe lung injury by zinc oxide nanoparticles; the role of Zn2+ dissolution inside lysosomes. *Part Fibre Toxicol*. 2011;8(1):27.
48. Heng BC, Zhao X, Tan EC, et al. Evaluation of the cytotoxic and inflammatory potential of differentially shaped zinc oxide nanoparticles. *Arch Toxicol*. 2011;85(12):1517–1528.
49. Hanley C, Layne J, Punnoose A, et al. Preferential killing of cancer cells and activated human T cells using ZnO nanoparticles. *Nanotechnology*. 2008;19(29):295103.
50. Kwon JY, Koedrith P, Seo YR. Current investigations into the genotoxicity of zinc oxide and silica nanoparticles in mammalian models in vitro and in vivo: carcinogenic/genotoxic potential, relevant mechanisms and biomarkers, artifacts, and limitations. *Int J Nanomedicine*. 2014; 9 Suppl 2:271–286.
51. Pujalté I, Passagne I, Brouillaud B, et al. Cytotoxicity and oxidative stress induced by different metallic nanoparticles on human kidney cells. *Part Fibre Toxicol*. 2011;8(10):1–16.
52. Wang Y, Ji P, Liu J, Broaddus RR, Xue F, Zhang W. Centrosome-associated regulators of the G2/M checkpoint as targets for cancer therapy. *Mol Cancer*. 2009;8(1):8.

53. Smerdon MJ, Tlsty TD, Lieberman MW. Distribution of ultraviolet-induced DNA repair synthesis in nuclease sensitive and resistant regions of human chromatin. *Biochemistry*. 1978;17(12):2377–2386.
54. Sidik K, Smerdon MJ. Nucleosome rearrangement in human cells following short patch repair of DNA damaged by bleomycin. *Biochemistry*. 1990; 29(32):7501–7511.
55. Huyen Y, Zgheib O, DiTullio Jr RA, et al. Methylated lysine 79 of histone H3 targets 53BP1 to DNA double-strand breaks. *Nature*. 2004; 432(7015):406–411.
56. Sanders SL, Portoso M, Mata J, Bähler J, Allshire RC, Kouzarides T. Methylation of histone H4 lysine 20 controls recruitment of Crb2 to sites of DNA damage. *Cell*. 2004;119(5):603–614.
57. Peterson CL, Côté J. Cellular machineries for chromosomal DNA repair. *Genes Dev*. 2004;18(6):602–616.
58. Tachibana M, Sugimoto K, Fukushima T, Shinkai Y. Set domain-containing protein, G9a, is a novel lysine-preferring mammalian histone methyltransferase with hyperactivity and specific selectivity to lysines 9 and 27 of histone H3. *J Biol Chem*. 2001;276(27):25309–25317.
59. Tachibana M, Ueda J, Fukuda M, et al. Histone methyltransferases G9a and GLP form heteromeric complexes and are both crucial for methylation of euchromatin at H3-K9. *Genes Dev*. 2005;19(7):815–826.
60. Colvin VL. The potential environmental impact of engineered nanomaterials. *Nat Biotechnol*. 2003;21(10):1166–1170.
61. Donaldson K, Tran L, Jimenez LA, et al. Combustion-derived nanoparticles: a review of their toxicology following inhalation exposure. *Part Fibre Toxicol*. 2005;2(1):10.
62. Li N, Sioutas C, Cho A, et al. Ultrafine particulate pollutants induce oxidative stress and mitochondrial damage. *Environ Health Perspect*. 2003;111(4):455.
63. Møller P, Jacobsen NR, Folkmann JK, et al. Role of oxidative damage in toxicity of particulates. *Free Radic Res*. 2010;44(1):1–46.
64. Albini A, Mussi V, Parodi A, et al. Interactions of single-wall carbon nanotubes with endothelial cells. *Nanomedicine*. 2010;6(2):277–288.
65. Yaron PN, Holt BD, Short PA, Losche M, Islam MF, Dahl KN. Single wall carbon nanotubes enter cells by endocytosis and not membrane penetration. *J Nanobiotechnol*. 2011;9(45):1–45.
66. De Berardis B, Civitelli G, Condello M, et al. Exposure to ZnO nanoparticles induces oxidative stress and cytotoxicity in human colon carcinoma cells. *Toxicol Appl Pharmacol*. 2010;246(3):116–127.
67. Kodiha M, Hutter E, Boridy S, Juhas M, Maysinger D, Stochaj U. Gold nanoparticles induce nuclear damage in breast cancer cells, which is further amplified by hyperthermia. *Cell Mol Life Sci*. 2014;71(21): 4259–4273.
68. Dam DHM, Lee JH, Sisco PN, et al. Direct observation of nanoparticle–cancer cell nucleus interactions. *ACS Nano*. 2012;6(4):3318–3326.
69. Kang B, Mackey MA, El-Sayed MA. Nuclear targeting of gold nanoparticles in cancer cells induces DNA damage, causing cytokinesis arrest and apoptosis. *J Am Chem Soc*. 2010;132(5):1517–1519.